DE GRUYTER OPEN

Journal of ELECTRICAL ENGINEERING, VOL 68 (2017), NO6, 470–475

Fourier decomposition of segmented magnets with radial magnetization in surface-mounted PM machines

Tow Leong Tiang*, **Dahaman Ishak****, **Chee Peng Lim*****

This paper presents a generic field model of radial magnetization (RM) pattern produced by multiple segmented magnets per rotor pole in surface-mounted permanent magnet (PM) machines. The magnetization vectors from either odd- or even-number of magnet blocks per pole are described. Fourier decomposition is first employed to derive the field model, and later integrated with the exact 2D analytical subdomain method to predict the magnetic field distributions and other motor global quantities. For the assessment purpose, a 12-slot/8-pole surface-mounted PM motor with two segmented magnets per pole is investigated by using the proposed field model. The electromagnetic performances of the PM machines are intensively predicted by the proposed magnet field model which include the magnetic field distributions, airgap flux density, phase back-EMF, cogging torque, and output torque during either open-circuit or on-load operating conditions. The analytical results are evaluated and compared with those obtained from both 2D and 3D finite element analyses (FEA) where an excellent agreement has been achieved.

K e y w o r d s: Fourier decomposition, magnet segmentation, permanent magnet synchronous machine, radial magnetization

1 Introduction

The rare-earth magnet materials such as Neodymium Iron Boron (NdFeB) and Samarium Cobalt (SmCo) have been widely utilized in the production of surface-mounted permanent magnet synchronous machines (PMSMs). However, these high energy magnets tend to make the PMSMs suffer from excessive cogging torque and distorted phase back-EMF, resulting in undesired torque ripples and vibration which are detrimental to the overall performance and capability of the motor [1, 2]. One of the methods to suppress the torque vibration in PM machines is by segmenting the surface-mounted magnet into several magnet blocks per rotor pole [1, 3, 4]. Since 1992, many researchers have employed the Fourier series space decompositions to emulate different magnetization patterns in PMSMs, for example, prediction of motor performance due to the magnet fields with radial magnetization (RM) [5] and parallel magnetization (PaM) [6]. However, they only considered single magnet segment per rotor pole [5, 6]. Conversely, the analytical models of multiple segmented magnets per magnetic pole were reported in [7] and [8], but, the models were derived for various Halbach configurations. Additionally, the magnet field models were developed to emulate RM produced by several magnet blocks per rotor pole [1, 3, 4]. Nevertheless, the model reported by Lateb is derived based on an approximated Fourier coefficient [1], therefore, the magnetic field prediction is inaccurate. Also, the formulations of magnet field models that proposed by Ashabani [3] and Tiang [4] are complex since they superimpose a high number of virtual PM blocks in order to obtain the equivalent field distributions produced by multi-segmented magnets.

Therefore, this motivates us to investigate further on this topic. A field model based on Fourier series decomposition is considered here to represent the net effect of the magnetic field distributions produced by multi-segmented magnets mounted on the rotor surface in polyphase PMSMs. This is important because the analytical method can provide valuable information and physical insights of the machine performance during initial design stage.

2 Fourier series space decomposition of magnet segmentations for radial magnetization

The radial magnetization (RM) pattern produced by single magnet per pole is first considered, and its radial and tangential components, M_{r1} and $M_{\alpha 1}$, respectively, are illustrated in Fig. 1. In this case, the rotor positions, α_{r1} to α_{r4}, are indicated, α_{p1} is the magnet pole-pitch ratio, and p is the number of pole-pairs. Noted that the magnet pitch ratio of single magnet segment is solely determined by α_{p1}.

Table 1 describes the radial component of magnetization function with its rotor positions for RM pattern produced by single magnet segment per magnetic pole.

*Universiti Malaysia Perlis, Pauh Putra Campus, Arau, Perlis 02600, Malaysia, ** Universiti Sains Malaysia, Engineering Campus, Nibong Tebal, Penang 14300, Malaysia, dahaman@usm.my, *** Deakin University, Geelong Waurn Ponds Campus, Geelong, Victoria 3220, Australia

DOI: 10.1515/jee-2017–0082, Print (till 2015) ISSN 1335-3632, On-line ISSN 1339-309X

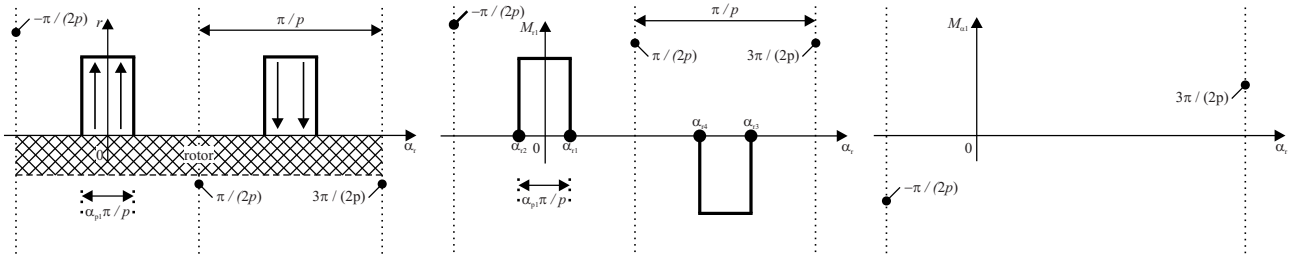

Fig. 1. Typical RM produced by single magnet segment per magnetic pole: (a) – magnetization pattern, (b) – radial magnetization component with its indicated rotor positions from α_{r1} to α_{r4}, (c) – tangential magnetization component

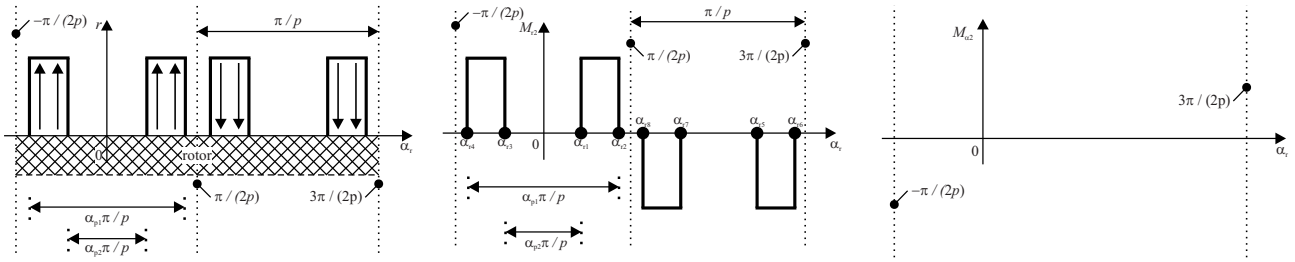

Fig. 2. Typical RM produced by two segmented magnets per magnetic pole: (a) – magnetization pattern, (b) – radial magnetization component with its indicated rotor positions from α_{r1} to α_{r8}, (c) – tangential magnetization

Table 1. Radial component of magnetization function with its rotor positions for RM pattern produced by single magnet segment per pole

M_{r1}	Rotor angular position
B_r/μ_0	$-\alpha_{p1}\pi/(2p) \le \alpha_r \le \alpha_{p1}\pi/(2p)$
$-B_r/\mu_0$	$(2-\alpha_{p1})\pi/(2p) \le \alpha_r \le (2+\alpha_{p1})\pi/(2p)$

5

The Fourier field model of RM pattern produced by single magnet segment per magnetic pole can be obtained in [2] and rewritten as below

$$M_{r1} = \sum\nolimits_{k=1,3,5,\ldots} M_{rck1}\cos(k\alpha) + M_{rsk1}\sin(k\alpha)\,, \quad (1)$$

$$M_{\alpha 1} = \sum\nolimits_{k=1,3,5,\ldots} M_{\alpha ck1}\cos(k\alpha) + M_{\alpha sk1}\sin(k\alpha)\,, \quad (2)$$

$$M_{rck1} = M_{rk1}\cos(k\omega_r t + k\alpha_0)\,, \quad (3)$$

$$M_{rsk1} = M_{rk1}\sin(k\omega_r t + k\alpha_0)\,, \quad (4)$$

$$M_{\alpha ck1} = -M_{\alpha k1}\sin(k\omega_r t + k\alpha_0)\,, \quad (5)$$

$$M_{\alpha sk1} = M_{\alpha k1}\cos(k\omega_r t + k\alpha_0) \quad (6)$$

where α_0 is the rotor position at initial location, ω_r is the angular speed of the rotor, M_{rk1} and $M_{\alpha k1}$ are the normal and circumferential components of magnetization vector with the k^{th} harmonic number for RM pattern produced by single magnet segment per pole. As can be seen in Fig. 1(c), the tangential component of magnetization vector is always zero, therefore, $M_{\alpha k1}$ is zero; meanwhile, M_{rk1} can be expanded into Fourier series as

$$M_{rk1} = \frac{pB_r}{\pi\mu_0}\left\{\int_{\alpha_{r2}}^{\alpha_{r1}} \cos(k\alpha_r)\mathrm{d}\alpha_r - \int_{\alpha_{r4}}^{\alpha_{r3}} \cos(k\alpha_r)\mathrm{d}\alpha_r\right\}$$
$$= \sum\nolimits_{k/p=1,3,5,\ldots} 4pB_r\sin(k\pi\alpha_{p1}/2p)/k\pi\mu_0\,, \quad (7)$$

$$M_{\alpha k1} = 0\,. \quad (8)$$

Next, the RM pattern produced by two segmented magnets per magnetic pole is considered and its radial and tangential components, M_{r2} and $M_{\alpha 2}$, respectively, are illustrated in Fig. 2. In this case, the rotor positions, α_{r1} to α_{r8}, are indicated, while α_{p1} and α_{p2} are the pitch ratios. Noted that the magnet spans are determined by the differences between α_{p1} and α_{p2}. The radial component of magnetization function with its rotor positions for RM pattern produced by two segmented magnets per magnetic pole is fully outlined in Tab. 2

Table 2. Radial component of magnetization function with its rotor positions for rm pattern produced by two segmented magnets per pole

M_{r2}	Rotor angular position
B_r/μ_0	$-\alpha_{p1}\pi/(2p) \le \alpha_r \le -\alpha_{p2}\pi/(2p)$
B_r/μ_0	$\alpha_{p2}\pi/(2p) \le \alpha_r \le \alpha_{p1}\pi/(2p)$
$-B_r/\mu_0$	$(2-\alpha_{p1})\pi/(2p) \le \alpha_r \le (2-\alpha_{p2})\pi/(2p)$
$-B_r/\mu_0$	$(2+\alpha_{p2})\pi/(2p) \le \alpha_r \le (2+\alpha_{p1})\pi/(2p)$

Therefore, the field model of RM pattern produced by two segmented magnets per magnetic pole can be obtained as

$$M_{r2} = \sum\nolimits_{k=1,3,5,\ldots} M_{rck2}\cos(k\alpha) + M_{rsk2}\sin(k\alpha)\,, \quad (9)$$

$$M_{\alpha 2} = \sum\nolimits_{k=1,3,5,\ldots} M_{\alpha ck2}\cos(k\alpha) + M_{\alpha sk2}\sin(k\alpha)\,, \quad (10)$$

$$M_{rck2} = M_{rk2}\cos(k\omega_r t + k\alpha_0)\,, \quad (11)$$

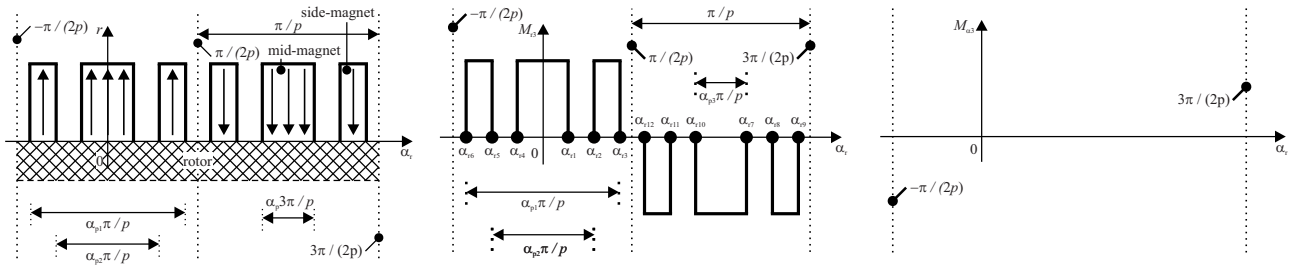

Fig. 3. Typical RM produced by three segmented magnets per magnetic pole: (a) – magnetization pattern, (b) – radial magnetization component with its indicated rotor positions from α_{r1} to α_{r12}, (c) – tangential magnetization component

$$M_{rsk2} = M_{rk2}\sin(k\omega_r t + k\alpha_0)\,, \tag{12}$$

$$M_{\alpha ck2} = -M_{\alpha k2}\sin(k\omega_r t + k\alpha_0)\,, \tag{13}$$

$$M_{\alpha sk2} = M_{\alpha k2}\cos(k\omega_r t + k\alpha_0) \tag{14}$$

where M_{rk2} and $M_{\alpha k2}$ are the normal and circumferential components of magnetization vector with the k^{th} harmonic number for RM pattern produced by two segmented magnets per pole. As can be seen in Fig. 2(c), the tangential component of magnetization vector is always zero, therefore, $M_{\alpha k2}$ is zero; meanwhile, M_{rk2} can be expanded into Fourier series as

$$M_{rk2} = pB_r/\pi\mu_0\Big\{\int_{\alpha_{r4}}^{\alpha_{r3}}\cos(k\alpha_r)\mathrm{d}\alpha_r + \int_{\alpha_{r1}}^{\alpha_{r2}}\cos(k\alpha_r)\mathrm{d}\alpha_r - \int_{\alpha_{r8}}^{\alpha_{r7}}\cos(k\alpha_r)\mathrm{d}\alpha_r - \int_{\alpha_{r5}}^{\alpha_{r6}}\cos(k\alpha_r)\mathrm{d}\alpha_r\Big\} = \sum_{k/p=1,3,5,\ldots}\frac{4pB_r}{k\pi\mu_0}\big[\sin(k\pi\alpha_{p1}/2p) - \sin(k\pi\alpha_{p2}/2p)\big], \tag{15}$$

$$M_{\alpha k2} = 0\,. \tag{16}$$

Following similar steps, the RM pattern produced by three segmented magnets per magnetic pole is now considered and its radial and tangential components, M_{r3} and $M_{\alpha 3}$, respectively, are illustrated in Fig. 3. In this case, the rotor positions, α_{r1} to α_{r12}, are indicated, while α_{p1}, α_{p2}, and α_{p3} are the pitch ratios. Noted that the magnet span of mid-magnet is determined by α_{p3}. Meanwhile, the magnet spans of side-magnets are determined by the differences between α_{p1} and α_{p2}. The radial component of magnetization function with its rotor positions for RM pattern produced by three segmented magnets per magnetic pole is given in Tab. 3, the Fourier field model of RM pattern produced by three segmented magnets per magnetic pole can be obtained as

$$M_{r3} = \sum\nolimits_{k=1,3,5,\ldots} M_{rck3}\cos(k\alpha) + M_{rsk3}\sin(k\alpha)\,, \tag{17}$$

$$M_{\alpha 3} = \sum\nolimits_{k=1,3,5,\ldots} M_{\alpha ck3}\cos(k\alpha) + M_{\alpha sk3}\sin(k\alpha)\,, \tag{18}$$

$$M_{rck3} = M_{rk3}\cos(k\omega_r t + k\alpha_0)\,, \tag{19}$$

$$M_{rsk3} = M_{rk3}\sin(k\omega_r t + k\alpha_0)\,, \tag{20}$$

$$M_{\alpha ck3} = -M_{\alpha k3}\sin(k\omega_r t + k\alpha_0)\,, \tag{21}$$

$$M_{\alpha sk3} = M_{\alpha k3}\cos(k\omega_r t + k\alpha_0) \tag{22}$$

where M_{rk3} and $M_{\alpha k3}$ are the normal and circumferential components of magnetization vector with the k^{th} harmonic number for RM pattern produced by three segmented magnets per pole.

Table 3. Radial component of magnetization function with its rotor positions for RM pattern produced by three segmented magnets per pole

M_{r3}	Rotor angular position
B_r/μ_0	$-\alpha_{p1}\pi/(2p) \le \alpha_r \le -\alpha_{p2}\pi/(2p)$
B_r/μ_0	$-\alpha_{p3}\pi/(2p) \le \alpha_r \le \alpha_{p3}\pi/(2p)$
B_r/μ_0	$\alpha_{p2}\pi/(2p) \le \alpha_r \le \alpha_{p1}\pi/(2p)$
$-B_r/\mu_0$	$(2-\alpha_{p1})\pi/(2p) \le \alpha_r \le (2-\alpha_{p2})\pi/(2p)$
$-B_r/\mu_0$	$(2-\alpha_{p3})\pi/(2p) \le \alpha_r \le (2+\alpha_{p3})\pi/(2p)$
$-B_r/\mu_0$	$(2+\alpha_{p2})\pi/(2p) \le \alpha_r \le (2+\alpha_{p1})\pi/(2p)$

As can be seen in Fig. 3(c), the tangential component of magnetization vector is always zero, therefore, $M_{\alpha k3}$ is zero; meanwhile, M_{rk3} can be expanded into Fourier series as

$$M_{rk3} = pB_r/\pi\mu_0\Big\{\int_{\alpha_{p6}}^{\alpha_{p5}}\cos(k\alpha_r)\mathrm{d}\alpha_r + \int_{\alpha_{p4}}^{\alpha_{p1}}\cos(k\alpha_r)\mathrm{d}\alpha_r + \int_{\alpha_{p2}}^{\alpha_{p3}}\cos(k\alpha_r)\mathrm{d}\alpha_r - \int_{\alpha_{p12}}^{\alpha_{p11}}\cos(k\alpha_r)\mathrm{d}\alpha_r - \int_{\alpha_{p10}}^{\alpha_{p7}}\cos(k\alpha_r)\mathrm{d}\alpha_r - \int_{\alpha_{p8}}^{\alpha_{p9}}\cos(k\alpha_r)\mathrm{d}\alpha_r\Big\} = \sum\nolimits_{k/p=1,3,5,\ldots} 4pB_r/k\pi\mu_0\big\{\sin(k\pi\alpha_{p1}/2p) - \sin(k\pi\alpha_{p2}) + \sin(k\pi\alpha_{p3}/2p)\big\}, \tag{23}$$

$$M_{\alpha k3} = 0\,. \tag{24}$$

Based on the Fourier series space decomposition to emulate the RM pattern produced by single magnet segment, two segmented magnets, and three segmented magnets per magnetic pole, the Fourier coefficients of $M_{\alpha k1}$, $M_{\alpha k2}$, and $M_{\alpha k3}$ are always zero. On the other hand, the Fourier coefficients of M_{rk1}, M_{rk2}, and M_{rk3} demonstrate a common and generic expression, which can be

Table 4. Main Parameters of 12s/8p Surface-Mounted PM Motor with 2SM per Pole

Parameters	Value	Parameters	Value
Slot number, N_s	12	Pole number, $2p$	8
Remanence, B_r (T)	1.12	Tooth-tips edge (mm)	3
Airgap length, l_g (mm)	1.0	Active length, l_a (mm)	50
Winding turns/coil, N_c	30	Stator yoke height (mm)	7.5
Bottom slots radius, R_{sb} (mm)	42.5	Magnet thickness, h_m (mm)	3
PM surface radius, R_m (mm)	26	Stator inner radius, R_s (mm)	50
Stator outer radius (mm)	50	Magnetization pattern	RM
Winding slot angle, b_{sa} (mech. deg.)	15	Rotor yoke inner radius, R_r (mm)	23
Slot-opening angle, b_{oa} (mech. deg.)	5.5	Relative recoil permeability,	1.5
σ_{p1} (elect. deg.)	147.6	σ_{p2} (elect. deg.)	11.2

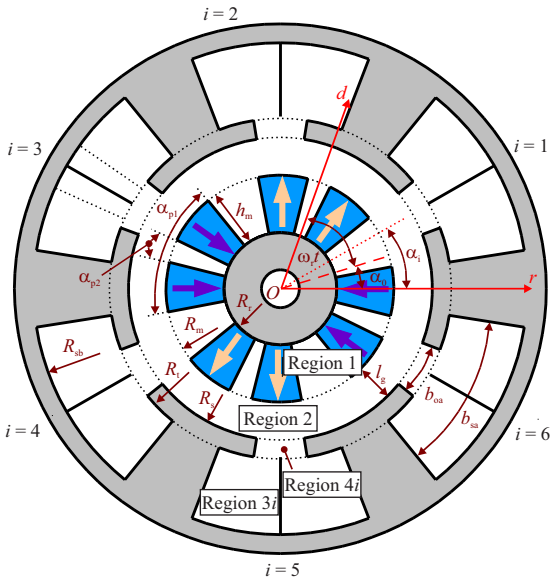

Fig. 4. A typical geometry and its symbols of a surface-mounted PMSM (Region 1, 2, $3i$, and $4i$ represent magnet, airgap, the i^{th} winding slot, and the i^{th} slot-opening

deduced for the v^{th} segmented magnets per pole as

$$M_{rk} = \sum_{\substack{\nu=1,2,3,\ldots \\ k/p=1,3,5,\ldots}} (-1)^{(v+1)} \frac{4pB_r}{k\pi\mu_0} \sin\frac{k\pi\alpha_{pv}}{2p}\,, \tag{25}$$

$$M_{\alpha k} = 0\,. \tag{26}$$

Also, the normal and tangential components of magnetization functions can be rewritten as

$$M_r = \sum\nolimits_{k=1,3,5,\ldots} M_{rck}\cos(k\alpha) + M_{rsk}\sin(k\alpha)\,, \tag{27}$$

$$M_\alpha = \sum\nolimits_{k=1,3,5,\ldots} M_{\alpha ck}\cos(k\alpha) + M_{\alpha sk}\sin(k\alpha)\,, \tag{28}$$

$$M_{rck} = M_{rk}\cos(k\omega_r t + k\alpha_0)\,, \tag{29}$$

$$M_{rsk} = M_{rk}\sin(k\omega_r t + k\alpha_0)\,, \tag{30}$$

$$M_{\alpha ck} = -M_{\alpha k}\sin(k\omega_r t + k\alpha_0)\,, \tag{31}$$

$$M_{\alpha sk} = M_{\alpha k}\cos(k\omega_r t + k\alpha_0)\,. \tag{32}$$

From here, the magneto-quasi Maxwell equations are solved using separable variables technique to compute the magnetic field in every subdomain [2], of a surface-mounted PMSM, as shown in Fig. 4. Several important assumptions are also considered as reported in [4]. Subsequently, the motor global quantities can be evaluated, *eg* the back-EMFs, cogging torque, and output torque, which can be found in [2].

3 Analysis and validations

In this paper, the proposed field model based on Fourier series space decomposition of RM pattern produced by multiple segmented magnets per pole is integrated with the 2D exact subdomain model [2, 4] to predict the magnetic fields in semi-closed surface-mounted PM machines. The magnetic field distributions and the motor global quantities that include phase back-EMF, cogging torque, and output torque of a three-phase, $12s/8p$ surface-mounted PMSM are then calculated by the analytical method. Meanwhile, 2D and 3D FEA for the PM motor are evaluated by employing a commercial FE software, *ie*, Cobham Vector Field Opera 2D/3D to validate the computed analytical results. The symbols of typical surface-mounted PM motor are displayed in Fig. 4, and the main parameters of $12s/8p$, three-phase, surface-mounted PM motor are given in Tab. 4.

Figure 5 shows the magnetic field distributions as predicted by the 2D and 3D FEA for the $12s/8p$ PM machine during open-circuit and on-load conditions. As can be seen in Figs. 5(a) and 5(c), the airgap spacings between the segmented magnets and magnet interpoles provide alternative flux paths among the PMs, instead of direct interaction between the magnets and stator teeth. The magnetic forces between magnets and slot-openings

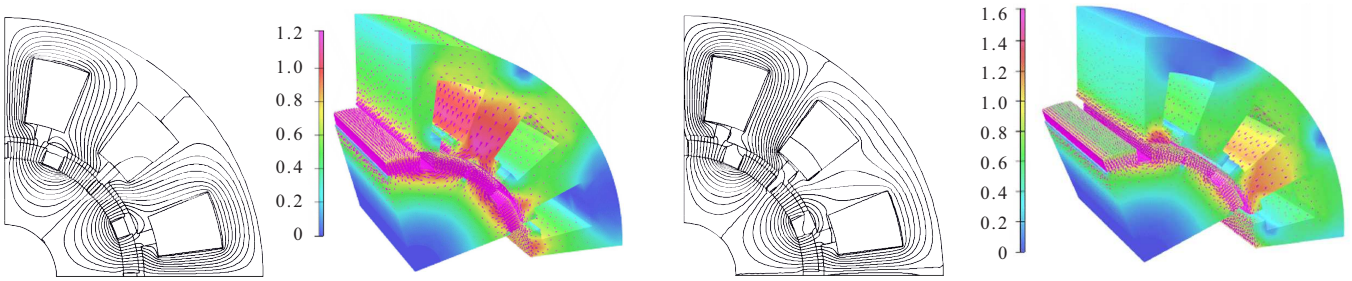

Fig. 5. Magnetic field distributions as predicted by FEA in $12s/8p$ PM machine with 2SM per pole during two operating conditions: (a) – 2D FEA (open-circuit), (b) – 3D FEA (open-circuit), (c) – 2D FEA (on-load), (d) – 3D FEA (on-load)

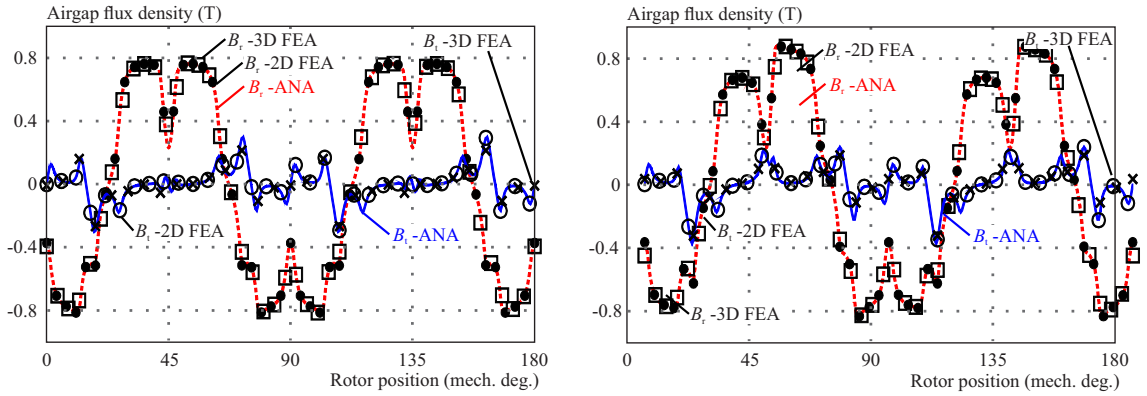

Fig. 6. Radial and tangential components of magnetic flux density in the mid-airgap ($r = 26.5$ mm) of $12s/8p$ PM machine with 2SM per pole predicted by the proposed Fourier field model, 2D FEA, and 3D FEA operating at different conditions: (a) – open-circuit, (b) – on-load

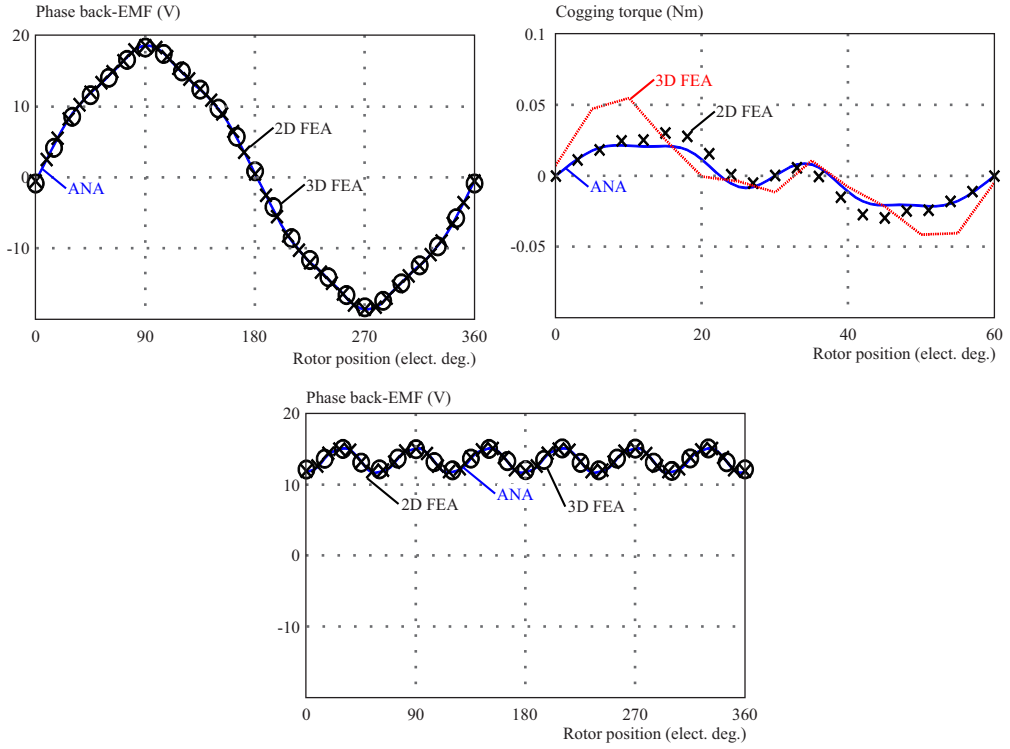

Fig. 7. Electromagnetic performances of $12s/8p$ PM machine with 2SM per pole predicted by the proposed Fourier field model, 2D FEA, and 3D FEA: (a) – phase back-emf, (b) – cogging torque, (c) – elctromagnetic torque

can be minimized by having multiple segmented magnets mounted on the rotor surface. Hence, smaller cogging torque is realized. Whereas, the magnetic field distributions in 3D model are shown in Figs. 5(b) and 5(d).

Furthermore, Fig. 6 shows the magnetic flux density distributions as predicted by the proposed Fourier field model in the mid-airgap ($r = 26.5$ mm) during open-circuit and on-load conditions, which are validated by the

2D and 3D FEA, for both radial and tangential components. An excellent agreement has been achieved.

Additionally, the predicted phase back-EMF, cogging torque, and output torque by the proposed model using Fourier series space decomposition are presented in Fig. 7. For the output torque computation, the motor has been excited with sinusoidal phase currents of 5A peak. They are also compared and verified with the 2D and 3D FEA respectively. All analytically predicted results have demonstrated a very good agreement with the FE simulated results. Therefore, the 2D and 3D FE simulated results confirm the effectiveness of the proposed field model.

4 Conclusion

This paper has presented a generic field model of radial magnetization (RM) pattern produced by multiple segmented magnets per rotor pole in surface-mounted permanent magnet (PM) machines. The rotor magnets can be formed by odd- or even-number of magnet blocks. Fourier decomposition is used to formulate the field model, and later integrated with the exact 2D analytical subdomain method to predict the magnetic field distributions and other motor quantities such as airgap flux density, phase back-EMF, cogging torque, and output torque during either open-circuit or on-load operating conditions. The analytical results are evaluated and compared with those obtained from both 2D and 3D finite element analyses (FEA) where an excellent agreement has been achieved.

Acknowledgements

The authors would like to express their gratitude and thank to Universiti Sains Malaysia and Ministry of Higher Education Malaysia for the financial support under grant number FRGS/1/2015/TK04/USM/02/1.

References

[1] R. Lateb, N. Takorabet and F. Meibody-Tabar, "Effect of Magnet Segmentation on the Cogging Torque Surface-Mounted Permanent-Magnet Motors", *IEEE Trans. Magn.*, vol. 42, pp. 442–445, 2006.

[2] L. J. Wu, Z. Q. Zhu, D. Staton, M. Popescu and D. Hawkins, "Analytical Prediction of Electromagnetic Performance of Surface-Mounted PM Machines based on Subdomain Model Accounting for Tooth-Tips", *IET Electric Power Applications*, vol. 5, pp. 597–609, 2011.

[3] M. Ashabani and Y. A. R. I. Mohamed, "Multiobjective Shape Optimization of Segmented Pole Permanent-Magnet Synchronous Machines with Improved Torque Characteristics", *IEEE Trans. Magn.*, vol. 47, pp. 795–804, 2011.

[4] T. L. Tiang, D. Ishak, C. P. Lim and M. R. Mohamed, "Analytical Method using Virtual PM Blocks to Represent Magnet Segmentations Surface-Mounted PM Synchronous Machines", *Progress Electromagnetics Research B (PIERB)*, vol. 76, pp. 23–36, 2017.

[5] Z. Q. Zhu and D. Howe, "Analytical Prediction of the Cogging Torque Radial-Field Permanent Magnet Brushless Motors", *IEEE Trans. Magn.* vol. 28, pp. 1371–1374, 1992.

[6] F. Dubas and C. Espanet, "Analytical Solution of the Magnetic Field Permanent-Magnet Motors Taking into Account Slotting Effect: No-Load Vector Potential Flux Density Calculation", *IEEE Trans. Magn.* vol. 45, pp. 2097–2109, 2009.

[7] Y. Shen and Z. Q. Zhu, "General Analytical Model for Calculating Electromagnetic Performance of Permanent Magnet Brushless Machines Having Segmented Halbach Array", *IET Electrical Systems Transportation*, vol. 3, pp. 57–66, 2013.

[8] Y. Shen and Z. Q. Zhu, "Analysis of Electromagnetic Performance of Halbach PM Brushless Machines Having Mixed Grade Unequal Height of Magnets", *IEEE Trans. Magn.* vol. 49, pp. 1461–1469, 2013.

Received 17 July 2017

Tow Leong Tiang received the BEng (Hons) degree in electrical engineering, the MSc in power systems and energy conversion, and the Ph.D. degree in electrical machines and drives from the Universiti Sains Malaysia, Nibong Tebal, Malaysia, in 2009, 2012, and 2017, respectively. He is currently a senior lecturer at the School of Electrical Systems Engineering, Universiti Malaysia Perlis. His current research interests include design of permanent magnet synchronous machine and renewable energy.

Dahaman Ishak received the BSc degree in electrical engineering from Syracuse University, Syracuse, NY, USA, the MSc degree in electrical power from the University of Newcastle Upon Tyne, Newcastle upon Tyne, UK, and the PhD degree from the University of Sheffield, Sheffield, UK, in 1990, 2001 and 2005 respectively. He is currently an Associate Professor with the School of Electrical and Electronic Engineering, Universiti Sains Malaysia, Penang, Malaysia. His current research interests include high-performance permanent magnet brushless machines, electrical drives, power electronic converters and renewable energy.

Chee Peng Lim received the BEE (Hons) degree from the University of Technology Malaysia, Johor Bahru, Malaysia, in 1992, and the MSc (Hons) degree in control systems engineering and the PhD degree from the University of Sheffield, Sheffield, UK, in 1993 and 1997, respectively. He is currently an Associate Professor with the Centre for Intelligent Systems Research, Deakin University, Geelong, VIC, Australia. His current research interests include computational intelligence, pattern classification, optimization, fault detection and diagnosis, condition monitoring, and decision support systems.